Terahertz spoof plasmonic coaxial microcavity

Zaihe Yu,[1] Zhen Gao,[2] Zhengyong Song,[2] and Zhuoyuan Wang[1,*]

[1]Ningbo Institute of Technology, Zhejiang University, Ningbo, China

[2]Division of Physics and Applied Physics, School of Physical and Mathematical Sciences, Nanyang Technological University, Singapore 637371, Singapore

*Corresponding author: zywang1981@163.com

Received 13 November 2013; revised 25 December 2013; accepted 18 January 2014; posted 22 January 2014 (Doc. ID 201245); published 14 February 2014

We theoretically demonstrate a subwavelength spoof surface-plasmon–polariton (SPP) microcavity on a planar metallic surface working at the terahertz regime with a high-quality factor and ultra-small mode volume. The microcavity is based on plasmonic and metamaterial notions, and it consists of an easy-to-manufacture circular aperture and a bell-shaped metallic core. It is shown that such a structure can sustain SPP eigenmodes whose fields are tightly trapped within the microcavity. Using the proposed structure, a total Q factor of 1000 (including losses from metals at low temperatures) and subwavelength mode volume of $0.00018(\lambda/2)^3$ can be achieved in the THz range for the fundamental surface-plasmonic eigenmode at room temperature. Moreover, the key figures of merit such as resonance frequency can be flexibly tuned by modifying the geometry of the microcavity, making it attractive for broad applications in filters, light sources, energy storage, and on-chip optical communications.

OCIS codes: (240.6680) Surface plasmons; (250.5403) Plasmonics.
http://dx.doi.org/10.1364/AO.53.001118

1. Introduction

Electromagnetic (EM) radiation in the terahertz (THz) range bridges a gap between the far-infrared (photonics) and the microwave (electronics) regimes and has great potential in a broad range of scientific and technological areas, such as medical diagnostics, sensing, security imaging, and communications [1]. With recent advances in THz source and detection techniques, the building of highly compact THz circuits has stood out as an important accomplishment. Compared with other THz optical waveguides such as dielectric wires [2], photonic crystal fibers [3], and low-index discontinuity waveguides [4], surface plasmon polariton (SPP) is one of the most promising approaches for transporting and manipulating THz waves down to a deep subwavelength scale, making it possible to design and produce highly integrated THz circuits [5]. However, due to the huge permittivity of metals in the THz regime, the high confinement of SPPs at flat metal surfaces cannot be achieved, making them not suitable for routing applications and manipulations. To solve this problem, the idea of tailoring the topography of a perfect conductor to allow the existence of surface waves with behavior resembling that of SPPs (dubbed spoof SPPs) at optical frequencies was discussed in the context of 2D hole lattices [6] and 1D groove arrays [7]. The existence of such spoof SPPs has recently been verified in the THz regimes [8]. After that, many designs of THz plasmonic waveguides carrying tightly confined EM modes with subwavelength transverse cross section have been suggested [9–14]. However, the spoof plasmonic resonant cavities working at THz frequency with a high-quality factor (related to the dissipation rate of photons confined to the cavity) and ultra-small mode volume (the electric field strength per photon) have not been paid sufficient attention by researchers. It is well known that the subwavelength microcavities represent a critical application that can exploit field

1559-128X/14/061118-06$15.00/0

compression to create ultrasmall mode volume devices, which provide the necessary functionalities needed to assemble fully operational THz plasmonic circuits. Although the THz waveguides can be used to construct waveguide ring resonators [13] that enable the routing of various frequencies to different output ports, it is difficult for such filtering systems to reduce the whole device size to subwavelength scale and achieve relative small radiation loss in the meanwhile. This makes SPPs restricted in many important applications, especially in the THz regimes where deep subwavelength optical device techniques will be critical for integrating THz photonic and electronic circuits on a same CMOS-compatible chip. Because the behavior of the spoof SPPs closely resembles that of the conventional SPPs at optical frequencies, it seems that the THz spoof plasmonic resonant cavities can be designed efficiently by directly borrowing ideas from their counterparts in the visible range [15].

In this paper, we theoretically demonstrate a subwavelength THz microcavity with not only a high-quality factor but also ultra-small mode volume, which is made by drilling a circular hole on the metallic surface with a bell-shaped core left inside. The proposed microcavity has a planar and monolithic structure, and it is easy to be manufactured. It is found that such a microcavity is able to simultaneously achieve an ultra-small mode volume ($0.00018(\lambda/2)^3$) and a significantly high Q factor (greater than 1000) in the THz regime for the fundamental spoof plasmonic microcavity eigenmode. The achieved Q factor is very close to the theoretical metal-loss-limited quality factor. The nearly ideal Q factor is attributed to the suppression and minimization of radiation and scattering loss by the proposed geometrical structure. We also demonstrate that frequency dependent transmission can be realized in a spoof SPP waveguide by breaking the waveguide and inserting the proposed microcavity in the middle as a filter.

2. Proposed Microcavity and Its Analysis

The proposed THz spoof SPP microcavity consists of a circular aperture and a bell-shaped metallic core inside the aperture, where the aperture and the core are obtained by drilling on a flat metal surface. In contrast with the whispering-gallery microcavities working in the visible and near-infrared regimes, the proposed microcavity is a planar and monolithic system and should not pose significant manufacturing problems. The basic structure of the microcavity is sketched in Fig. 1(a). The geometric parameters defining the circular hole are the depth, H, and the diameter, d. The bell-shaped metallic core in the bottom of the round hole has a height of h, and its peak is rounded with curvature radius r.

For the proposed microcavity, the lower part with height being h is a coaxial line without cut-off frequency, while the upper part with height being $h' = H - h$ is a metallic circular waveguide with a

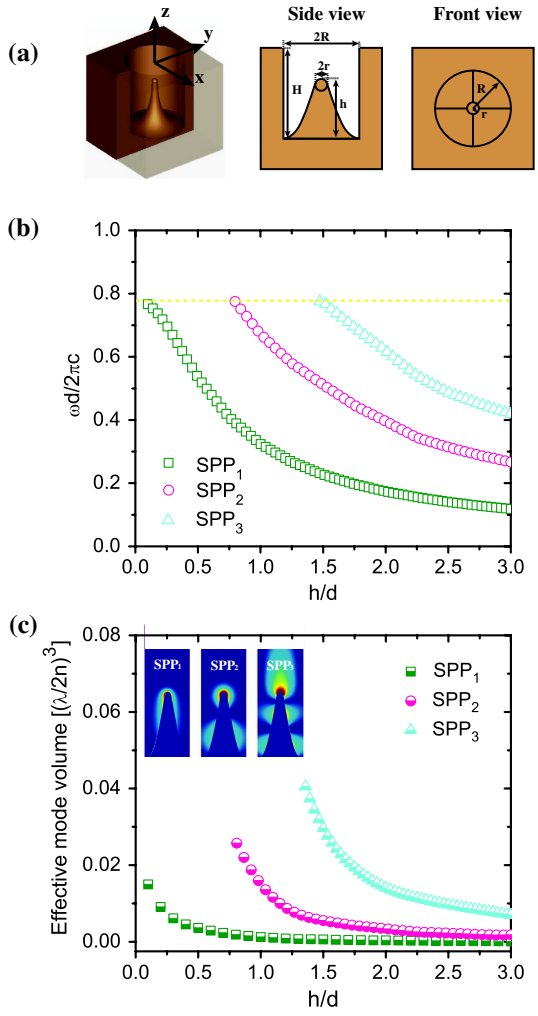

Fig. 1. (a) From left to right are, respectively, the 3D schematic, side view, and front view of the THz spoof plasmonic microcavity. The structure consists of an inner bell-shaped core and a circular aperture as a shield, both made of plasmonic metal (e.g., copper). H and d are, respectively, the depth and the diameter of the circular hole, and h and r are, respectively, the height and the curvature radius of rounded apex of the bell-shaped core. (b) The normalized resonance frequency as functions of h for the three lowest-order eigenmodes of the microcavity with $H = 3d$, $r = 0.05d$, and $d = 100$ μm. The yellow dashed line indicates the normalized cut-off frequency of the circular waveguide in the upper part of the microcavity. (c) The effective mode volume of the three-lowest eigenmodes of the microcavity versus h for the microcavity as described in (b). Insets show the fundamental (first-), second-, and third-order eigenmodes (SPP_m) of the cavity for the case of $h = 1.5d$.

certain cut-off frequency (denoted by f_c). When the resonance frequency of the microcavity is below f_c, the upper part acts as a bandgap mirror, thus the energy is confined in the coaxial part (i.e., the lower part) of the microcavity. On the other hand, when the resonance frequencies of the spoof plasmonic microcavity eigenmodes are above f_c, the energy will elapse through the circular waveguide into the free space and the microcavity modes will disappear. This means that the mode number for this THz microcavity is finite, where the mode number is defined

as the number of antinodes in the absolute electric field along the bell-shaped core (i.e., z direction).

To gain physical insight, we first model the metal as a perfect electric conductor (PEC), which is an excellent approximation for real metal in the THz regime. Full vectorial finite element analysis has been performed for the THz spoof plasmonic microcavity by using commercial software (i.e., COMSOL Multiphysics). It should be noted that, as we are considering the PEC approximation, all magnitudes of the geometrical parameters and resonance frequencies of this THz spoof plasmonic cavity are scalable, and we thus take the circular aperture's diameter d as a unit length.

Figure 1(b) shows the cavity mode dispersion diagram of a THz spoof plasmonic microcavity with $H = 3d$ and $r = 0.05d$, where the horizontal axis corresponds to the height of the bell-shaped core, and the vertical axis corresponds to the real part of the normalized resonance frequency of the cavity modes. The simulation results for the first-order, second-order, and third-order cavity modes are plotted using green squares, pink circles, and blue triangles, respectively. The results for the resonance frequencies of the cavity modes as shown in Fig. 1(b) indicate that the proposed microcavity is able to support THz wave eigenmodes if its geometrical parameters are properly selected. For this type of cavity, the resonant condition has the form of $2k_0h + \pi + \phi_m = 2n\pi$, where n is the mode orders, $k_0 = \omega/c$ is the wavenumber in vacuum, and ϕ_m is the reflection phase from the upper circular waveguide. It is evident that the normalized resonance frequency closely depends on the core height h (i.e., monotonously decreasing with h). For the microcavity studied herein, the normalized cut-off frequency (TM_{01} mode) f_c of the metallic circular waveguide is about 0.7655 and is indicated using the yellow dashed line in Fig. 1(b).

The mode volume V_m is one of the key parameters for a microcavity, which is defined as the ratio of total electric field energy to the maximum of the electric field energy density, i.e., $V_m = (\int_V \varepsilon(\mathbf{r})|\mathbf{E}(\mathbf{r})|^2 d^3\mathbf{r}/\max[\varepsilon(\mathbf{r})|\mathbf{E}(\mathbf{r})|^2])$, where $\varepsilon(\mathbf{r})$ and $\mathbf{E}(\mathbf{r})$ are, respectively, the dielectric constant and the electric field strength at a point with the 3D coordinate being $\mathbf{r}$, and V is a quantization volume encompassing the microcavity and with boundaries in the radiation zone of the cavity mode under study. The effective mode volume, $\bar{V}_{\text{eff}}$, is the mode volume V_m normalized to $(\lambda/2)^3$, where λ is the vacuum wavelength in the material. In Fig. 1(c), the effective mode volumes of the three lowest-order spoof plasmonic microcavity eigenmodes are plotted as functions of the height of the bell-shaped core, h. As expected, the mode volume for a same eigenmode will continuously and quickly decrease as the height h is increased, and a lower-order eigenmode will have a smaller mode volume for the same value of h. Moreover, it is observed that the normalized mode volume and resonance frequency will keep unchanged when the cavity size is proportionally scaled. This means both of them can be easily scaled to other frequency regimes. In the insets of Fig. 1(c), we have also shown the simulation results for the absolute electric field amplitude on the plane that halves the microcavity vertically. It is evident that the spoof plasmonic microcavity eigenmodes have absolute electric field profiles that peak at the apex of the bell-shaped core.

It should be noted that, in Figs. 1(b) and 1(c), the notation SPP_m ($m = 1, 2$, or 3) stands for a SPP mode with mode number being m. Moreover, as higher-order modes have larger mode volume, we will only consider the fundamental eigenmode, which owns the most superior properties and promising applications in the rest of this paper.

In order to gain further insight into the underlying physics of the proposed microcavity structure, the electric and magnetic field amplitude distributions of the fundamental eigenmode (i.e., first-order eigenmode) are analyzed via simulations. Figure 2 depicts the calculated mode profile for a typical microcavity structure with $H = 2d$, $h = 1.5d$, and $r = 0.05d$, where d is chosen as 100 μm in simulations.

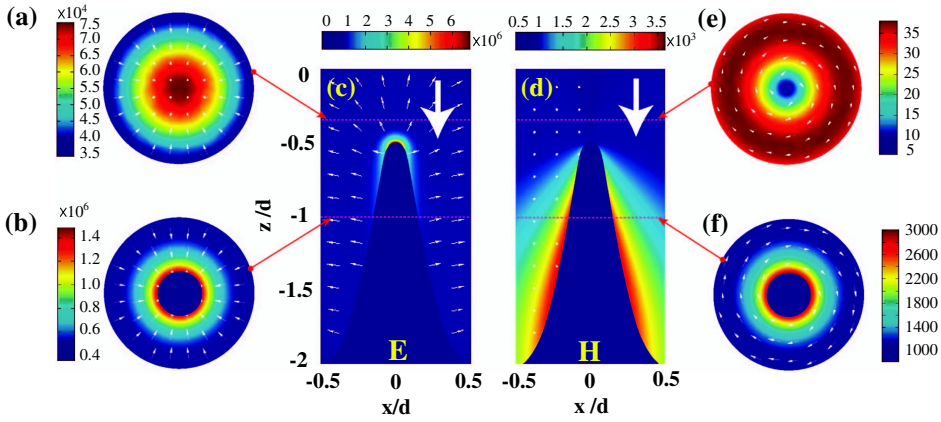

Fig. 2. Electric and magnetic field intensity distributions of the fundamental eigenmode in a microcavity with $d = 100$ μm, $H = 300$ μm, $r = 5$ μm, and $h = 150$ μm. (a) Electric field and (e) magnetic field on the plane of $z = -30$ μm. (b) Electric field and (f) magnetic field of coaxial mode on the plane of $z = -100$ μm plane. (c) Electric field and (d) magnetic field on the plane that halving the microcavity vertically. The small white arrows indicate the orientation of the field, and the big white arrow indicates the direction of the input field.

Panels (c) and (d) indicate the longitudinal cross sections (i.e., $x-z$ plane) of the electric field amplitude and the magnetic field amplitude, respectively. Panels (a) and (b), respectively, show the transverse cross sections (i.e., x-y plane) of the electric field amplitude at $z = -0.3d$ and $z = -d$, and panels (e) and (f) show the magnetic field amplitude distributions on the corresponding planes. The smaller white arrows represent the field orientation, and the bigger white arrows indicate the orientation of the input field. Evidently, the mode in the main part (i.e., the lower part) of the cavity is a typical coaxial mode without cut-off frequency, and the field in the upper part of the microcavity is a TM_{01} mode of metallic circular waveguide that is evanescent. The decay length of the evanescent wave with mode frequency being f is defined as $l' = c/2\pi\sqrt{f_c^2 - f^2}$. As demonstrated in the next paragraph, when the upper part's length h' is much greater than the decay length l', the radiation loss through the opening of the circular waveguide becomes negligible. This means the field energy will be tightly confined in the microcavity. For the microcavity studied here, h' is equal to $0.5d$, and l' for the fundamental eigenmode is about $0.2d$ [see B in Fig. 3(a)]. Since the fundamental eigenmode satisfies $h' > l'$, it should be confined in the microcavity. This has been confirmed by Fig. 2.

In addition to the resonance frequency and the effective mode volume, the quality factor (denoted by Q) is also an important parameter for plasmon resonance. A higher-quality factor is often desirable, as it means sharper resonance that leads to stronger local-field enhancement. The radiation quality factor is defined as $Q_{\text{rad}} = \omega(\int_V W(\mathbf{r})\mathrm{d}^3\mathbf{r}/P_r)$, where $W(\mathbf{r}) = (1/2)[\varepsilon(\mathbf{r})|\mathbf{E}(\mathbf{r})|^2 + \mu(\mathbf{r})|\mathbf{H}(\mathbf{r})|^2]$ is the total energy density, ω is the angular frequency of the mode, and P_r is the radiation loss energy. In the following, we will examine the influence of the geometrical parameters of the microcavity on the radiation quality factor. The radiation quality factor can be found by modeling the metals as PEC in computer simulations and thereby removing the resistive metallic loss. A perfectly matched layer (PML) is used to absorb all radiation from the cavity [16] in simulations. The simulation results for the dependence of Q_{rad} on h' are shown in Fig. 3(a), where the decay length values for $h = 2d$, $h = 1.5d$, $h = d$, and $h = 0.5d$ are marked using A, B, C, and D, respectively. It can be observed that Q_{rad} is heavily dependent on h', and its value rises quickly as h' is increased. An ultrahigh radiation quality factor can be easily achieved when the parameter h' is larger than the decay length. This is because when h' is significantly larger than the decay length, the modal fields will be well confined in the cavity, and the radiation loss through the opening of the upper circular waveguide will become negligible. On the other hand, the dependence of Q_{rad} on the parameter r is weaker. This is illustrated by the relationship between Q_{rad} and r for a microcavity with $H = 2d$ and $h = 1.5d$, which is shown in Fig. 3(b) using the green dotted line.

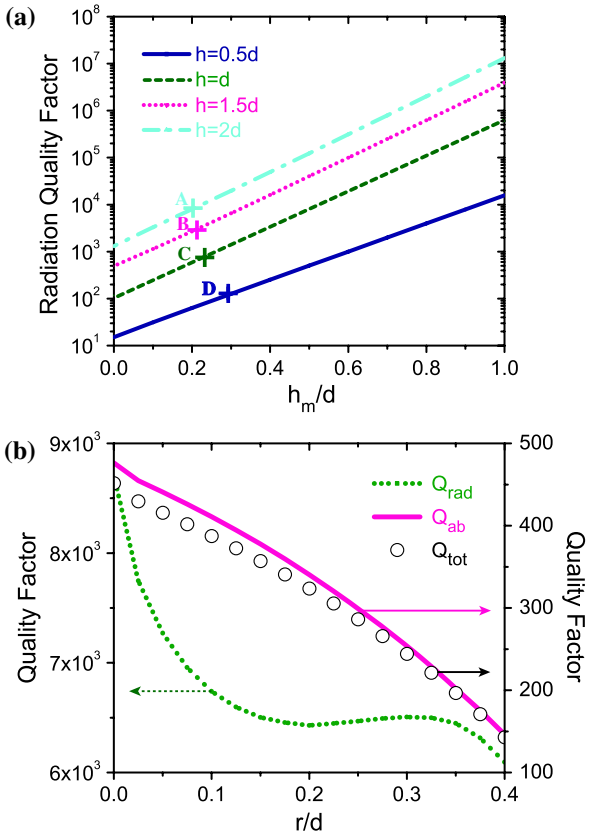

Fig. 3. (a) Dependence of radiation quality factor on the parameter h' under different values of bell-shaped core height h. The horizontal coordinates of the plus signs labeled with A, B, C, and D correspond to the decay length values of the resonance frequencies for $h = 2d$, $h = 1.5d$, $h = d$, and $h = 0.5d$, respectively. The other parameters of the microcavity are $d = 100$ μm and $r = 5$ μm. (b) The absorption quality factor (pink solid line), radiation quality factor (green dotted line), and total quality factor (black circles) as functions of the radius of curvature of the bell-shaped core r, where the other parameters of the microcavity are $h' = 50$ μm, $h = 150$ μm, and $d = 100$ μm.

In the above analysis, the metal is modeled as a PEC; thus the eigenmodes sustained by the THz microcavity are lossless. However, the loss of spoof SPPs is actually remarkable at THz frequencies when they are strongly confined [17,18]. To validate the effectiveness of our proposed structure in term of quality factor, we now consider a realistic cavity model at THz frequencies and examine the attenuation behavior of the fundamental eigenmode due to the absorption loss in the metal with finite conductivity. In order to make the microcavity operate in the THz region, we choose the diameter of the round hole as $d = 100$ μm. The metal is considered to be copper (Cu), and its dielectric properties are modeled using the Drude model with the parameters taken from [19]. We use a perturbation approach [20] to evaluate the metal-loss quality factor $Q_{\text{ab}} = \omega(\int_V W(\mathbf{r})\mathrm{d}^3\mathbf{r}/P_d)$, where P_d is the power dissipated in the metal. The total Q factor (denoted by Q_{tot}) is then calculated directly from the energy distribution, i.e.,

$Q_{tot}^{-1} \approx Q_{ab}^{-1} + Q_{rad}^{-1}$. That is, Q_{tot} includes contributions from intrinsic metal loss and geometry-dependent radiation loss through the hole opening. The simulation results of Q_{ab}, Q_{rab}, and Q_{tot} are, respectively, shown in Fig. 3(b) using pink line, green dotted line, and black circles, where the other parameters are $H = 200$ μm and $h = 150$ μm. It can be seen that the Q factor of this THz spoof SPP microcavity is metal-loss limited, i.e., $Q_{tot} \approx Q_{ab}$. This is because the microcavity has an ultrahigh radiation quality factor (i.e., Q_{rab}), which is larger than the metal-loss-limited Q factor (i.e., Q_{ab}) by several orders, making the contribution of Q_{rab} to Q_{tot} negligible. From Fig. 3(b), it can also be observed that both the metal-absorption quality factor Q_{ab} and the total quality factor Q_{tot} decreases as the radius of curvature of the bell-shaped core (i.e., r) grows. This can be explained by the field distributions in Fig. 2, where the bulk of the mode energy is distributed near the metallic core. As the value of r is increased, the core side area will become larger. Accordingly, the absorption power (i.e., P_{ab}) will increase, leading to smaller Q_{tot} and Q_{ab}. It should be noted that the quality factor can be further improved by using metals such as silver (Ag) or gold (Au), which have lower loss coefficients, or by optimizing the cavity design and mode profiles. Additionally, our numerical analysis shows that the total quality factor increases as the diameter of the microcavity d grows, and total Q factor of 1000 and subwavelength mode volume of $0.00018(\lambda/2)^3$ can be achieved in the THz range for the fundamental spoof plasmonic microcavity eigenmodes when the parameters of the spoof SPP microcavity are $d = 300$ μm, $H = 2d$, $h = 1.5d$, and $r = 5$ μm, respectively.

Now we turn to demonstrate that frequency-dependent transmission can be realized by using the proposed microcavity. For this purpose, we consider a filtering system based on the proposed microcavity and a spoof SPP waveguide, where the spoof SPP waveguide consists of a single row of rectangle holes periodically drilled into a flat metal surface. The spoof SPP waveguide is broken by removing three holes, and the proposed microcavity is placed in the middle of the removed area. To analyze the wave transmission through such a spoof SPP waveguide, we perform numerical simulations using the finite element method (FEM). In order to evaluate the transmission purely associated with the THz microcavity, the metal is approximated as PEC in the simulations. Figure 4(a) shows the transmission spectrum of the filter system. Figures 4(b)–4(d) show the simulation results for the absolute electric field amplitude on the plane located at $z = 2$ μm above the top of the waveguide, where the input wave frequencies for Figs. 4(b)–4(d) are $f = 0.88$ THz, $f = 0.91$ THz, and $f = 0.94$ THz, respectively. In the simulated system, the geometrical parameters of the used THz spoof plasmonic microcavity are $d = 150$ μm, $H = 100$ μm, $r = 5$ μm, and $h = 100$ μm. With the above parameters, the resonance frequency of the THz plasmonic microcavity is found to be $f \approx 0.91$ THz. The results as shown in Figs. 4(a) and 4(c) indicate that the amplitude transmissivity at the resonance frequency of the microcavity is very large (about 85%). In fact, nonnegligible radiation loss (about 15% of the input power) only occurs at the microcavity in the middle of the broken spoof SPP waveguide, and it is reasonably small since no optimization was attempted. On the other hand, as demonstrated in Figs. 4(b) and 4(d), the values of the amplitude transmissivity for inputs with frequencies not equal to the resonance frequency are very small (less than 10%), which match well with the transmission spectrum of this filter system as shown in Fig. 4(a). It can be predicted that, if design optimization is performed, the transmissivity for an input with frequency not equal to the resonance frequency can be further suppressed toward zero. In a word, frequency-dependent

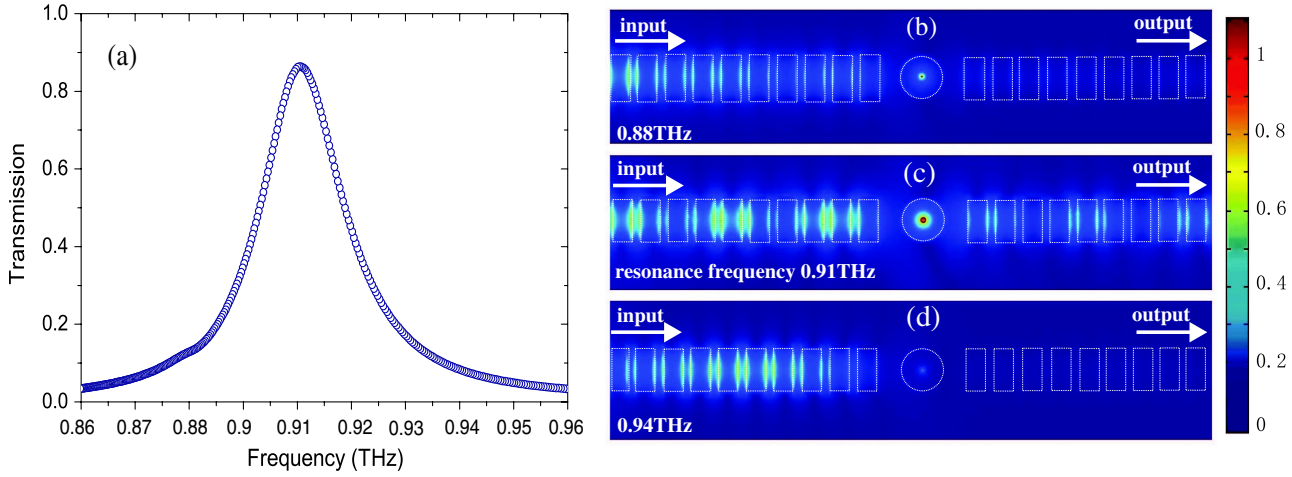

Fig. 4. (a) Transmission spectrum of the proposed filter system. Electric field amplitude distribution on a horizontal plane, which is 2 μm above the microcavity and waveguide along the z direction, where the input frequencies are (b) $f = 0.88$ THz, (c) $f = 0.91$ THz (resonance frequency of the microcavity), and (d) $f = 0.94$ THz frequency, respectively.

transmission has been achieved in the broken spoof SPP waveguide containing the proposed microcavity.

3. Conclusions

In summary, we have presented a new THz spoof plasmonic microcavity consisting of a bell-shaped metallic core within a circular aperture drilled on a flat metallic surface. The proposed microcavity is able to achieve an ultrahigh radiation quality factor, making its total quality factor close to the theoretical metal-loss-limited Q factor. It possesses subwavelength-scale physical size and extremely small mode volume. Moreover, the microcavity's resonance frequency, mode volume, and quality factor are all controlled by its geometrical parameters, which can be tuned at will. We have also shown that frequency-dependent transmission can be achieved in a filtering system based on the proposed microcavity and a broken spoof SPP waveguide. The proposed subwavelength microcavity can be used as filters or couplers, and it may find plenty of applications in the miniaturization and integration of THz optical components.

This work was supported by Natural Science Foundation of Ningbo (nos. 2013A610004 and 2011A610105) and NSFC grant 61275183.

References

1. M. Tonouchi, "Cutting-edge terahertz technology," Nat. Photonics **1**, 97–105 (2007).
2. S. P. Jamison, R. W. McGowan, and D. Grischkowsky, "Single-mode waveguide propagation and reshaping of sub-ps terahertz pulses in sapphire fibers," Appl. Phys. Lett. **76**, 1987–1989 (2000).
3. H. Han, H. Park, M. Cho, and J. Kim, "Terahertz pulse propagation in a plastic photonic crystal fiber," Appl. Phys. Lett. **80**, 2634–2636 (2002).
4. M. Nagel, A. Marchewka, and H. Kurz, "Low-index discontinuity terahertz waveguides," Opt. Express **14**, 9944–9954 (2006).
5. S. A. Maier, *Plasmonics-Fundamentals and Applications* (Springer, 2007).
6. J. B. Pendry, L. Martin-Moreno, and F. J. García-Vidal, "Mimicking surface plasmons with structured surfaces," Science **305**, 847–848 (2004).
7. F. J. García-Vidal, L. Martin-Moreno, and J. B. Pendry, "Surfaces with holes in them: new plasmonic metamaterials," J. Opt. A **7**, 97–107 (2005).
8. C. R. Williams, S. R. Andrews, S. A. Maier, A. I. Fernández-Domínguez, L. Martín-Moreno, and F. J. García-Vidal, "Highly confined guiding of terahertz surface plasmon polaritons on structured metal surfaces," Nat. Photonics **2**, 175–179 (2008).
9. S. A. Maier, S. R. Andrews, L. Martin-Moreno, and F. J. García-Vidal, "Terahertz surface plasmon-polariton propagation and focusing on periodically corrugated metal wires," Phys. Rev. Lett. **97**, 176805 (2006).
10. A. I. Fernandez-Dominguez, C. R. Williams, F. J. Garcia-Vidal, L. Martin-Moreno, S. R. Andrews, and S. A. Maier, "Terahertz surface plasmon polaritons on a helically grooved wire," Appl. Phys. Lett. **93**, 141109 (2008).
11. A. I. Fernandez-Dominguez, E. Moreno, L. Martin-Moreno, and F. J. Garcia-Vidal, "Guiding terahertz waves along subwavelength channels," Phys. Rev. B **79**, 233104 (2009).
12. A. I. Fernandez-Dominguez, E. Moreno, L. Martin-Moreno, and F. J. Garcia-Vidal, "Terahertz wedge plasmon polaritons," Opt. Lett. **34**, 2063–2065 (2009).
13. D. Martin-Cano, O. Quevedo-Teruel, E. Moreno, L. Martin-Moreno, and F. J. Garcia-Vidal, "Waveguided spoof surface plasmons with deep-subwavelength lateral confinement," Opt. Lett. **36**, 4635–4637 (2011).
14. G. Zhen, Z. Xufeng, and S. Linfang, "Wedge mode of spoof surface plasmon polaritons at terahertz frequencies," J. Appl. Phys. **108**, 113104 (2010).
15. E. Feigenbaum and M. Orenstein, "Ultrasmall volume plasmons, yet with complete retardation effects," Phys. Rev. Lett. **101**, 163902 (2008).
16. J. P. Berenger, "A perfectly matched layer for the absorption of electromagnetic waves," J. Comput. Phys. **114**, 185–200 (1994).
17. L. F. Shen, X. D. Chen, Y. Zhong, and K. Agarwal, "Effect of absorption on terahertz surface plasmon polaritons propagating along periodically corrugated metal wires," Phys. Rev. B **77**, 075408 (2008).
18. L. F. Shen, X. D. Chen, and T. J. Yang, "Terahertz surface plasmon polaritons on periodically corrugated metal surfaces," Opt. Express **16**, 3326–3333 (2008).
19. M. A. Ordal, L. L. Long, R. J. Bell, S. E. Bell, R. R. Bell, R. W. Alexander, Jr., and C. A. Ward, "Optical properties of the metals Al, Co, Cu, Au, Fe, Pb, Ni, Pd, Pt, Ag, Ti and W in the infrared and far infrared," Appl. Opt. **22**, 1099–1119 (1983).
20. J. A. Kong, *Electromagnetic Wave Theory* (EMW, 2005).